Supporting Information

Stimuli Responsive Behaviour in a D-A-D Organic Fluorophore: The Role of Cold Crystallization

Mohammad Afsar Uddin,[a,] Sergio Gámez-Valenzuela,[b] M. Carmen Ruiz Delgado,[b,]* and Berta Gómez-Lor, [a,]**

[a] *Instituto de Ciencia de Materiales de Madrid. CSIC. C/ Sor Juana Inés de la Cruz, 3, 28049. Madrid, Spain.*

[b] *Department of Physical Chemistry. University of Malaga. Campus de Teatinos s/n, Málaga, 29071, Spain*

List of contents **Page**

1. Experimental details

1.1. General

Nuclear Magnetic Resonance (NMR) characterization: ^{1}H-NMR and ^{13}C-NMR spectra were recorded on a Bruker AC 300 spectrometer (^{1}H 500 MHz; ^{13}C 75 MHz) spectrometer at 298 K using partially deuterated solvents as internal reference. Coupling constants (*J*) are denoted in Hz and chemical shifts (d in ppm. Multiplicities are denoted as: s = singlet, d = doublet, t = triplet, m = multiplet, br = broad). chemical shifts (δ) are quoted in parts per million,
Linear Spectroscopy: UV-Visible studies were carried out on a Varian Cary 5000 spectrophotometer. Fluorescence spectra were recorded on an Edinburgh Instruments FLS920 fluorometer.

Fluorescence quantum yield: The absolute quantum yield was registered in an Edinburgh Instruments FLS920 fluorometer, equipped with an integrating sphere, using a 450W Xe lamp as excitation source and the supplied blanking plug as blank sample.

Raman spectra: Raman spectra were recorded by using the 1x1 camera of a Bruker Senterra dispersive Raman microscope equipped with a CCD camera operating at -50ºC, a confocal microscope with a x40 objective, a neon lamp and a Nd:YAG laser working at λ=785 nm. This set up has a spectral resolution of 3-5 cm^{-1}. The power of the laser beam was kept at a level of 10 mW in all cases. The final spectrum is calculated as the average between 10 spectra of 10 seconds each to optimize the signal-to-noise ratio. The temperature of the sample was controlled by a Linkam temperature stage (BCS196). It was necessary to wait around 15 minutes for the sample to achieve a uniform temperature.

FT-IR spectra: FT-IR spectra were recorded with a Golden Gate Single Reflection Diamond ATR System (Graseby Specac) fitted into a Bruker Vertex 70 FT-IR spectrometer. The infrared spectra were collected with a standard spectral resolution of 4 cm^{-1}. The final spectrum is calculated as the average between 5 spectra of 64 scans each with the aim to obtain a high signal to noise ratio. Variable-temperature FT-IR measurements were carried out by using a Golden GateTM accessory coupled to the ATR System. It was necessary to wait around 15 minutes for the sample to achieve a uniform temperature.

Powder X-ray diffraction: Powder X-ray diffraction (PXRD) patterns were measured with a Bruker D8 diffractometer, with step size = 0.02° and exposure time = 0.5 s/step.

X-ray diffraction: Crystal of **DTBTE** was solved in a XtaLAB Synergy R, HyPix-Arc 100 diffractometer

Differential Scanning Calorimetry (DSC): DSC curves were recorded on a TA Instruments Discovery DSC calorimeter, utilizing standard TzeroTM sample holders. The purge gas used was N_2 at a flow rate of 50 mL/min, and a heating ramp of 10ºC/min from -10 °C to 180 °C was applied.

1.2. Synthesis and characterization

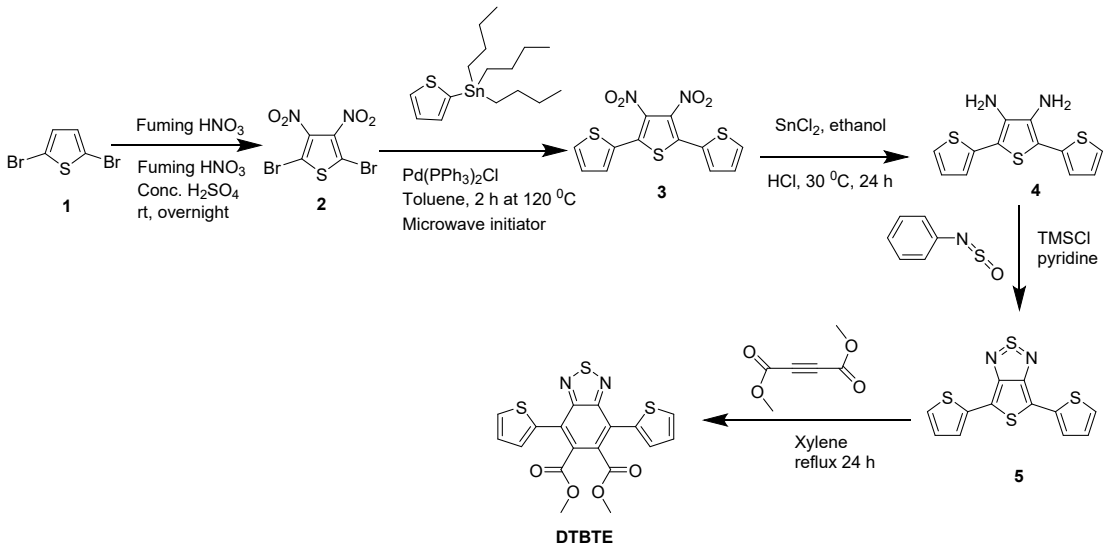

Scheme S1. Synthesis scheme of **DTBTE**.

Compounds 2-5 were synthesized according to literature.[1]

Dimethyl-4,7-di(2-thienyl)-2,1,3-benzothiadiazole-5,6-dicarboxylate (**DTBTE**, compound 1): Under an inert condition, dimethyl acetylenedicarboxylate (1.73 g, 12.17 mmol) was slowly added to a solution of o-xylene (60 mL) and 4,6-di(2-thienyl)-thieno[3,4-c][1,2,5]-thiadiazole (1.86 g, 6.06 mmol), and the mixture was refluxed. TLC monitoring (chloroform) showed complete consumption of the starting material after 5 hours. The reaction mixture was then concentrated with a rotary evaporator and crude brown solid obtained was loaded onto silica gel, eluted with chloroform, and further purified by recrystallization from methanol, to yield brown crystals (**DTBTE**) (2.00 g, 5.06 mmol, 83% yield)). ^{1}H NMR ($CDCl_3$) δ(ppm): 7.62 (dd, 2H), 7.45 (dd, 2H), 7.22 (dd, 2H), 3.79 (s, 6H); ^{13}C NMR ($CDCl_3$) δ(ppm): 168.0, 153.6, 135.0, 132.0, 129.7, 128.9, 127.2, 126.2 and 53.0.

1.3. Copy of ^{1}H-NMR and ^{13}C-NMR spectra

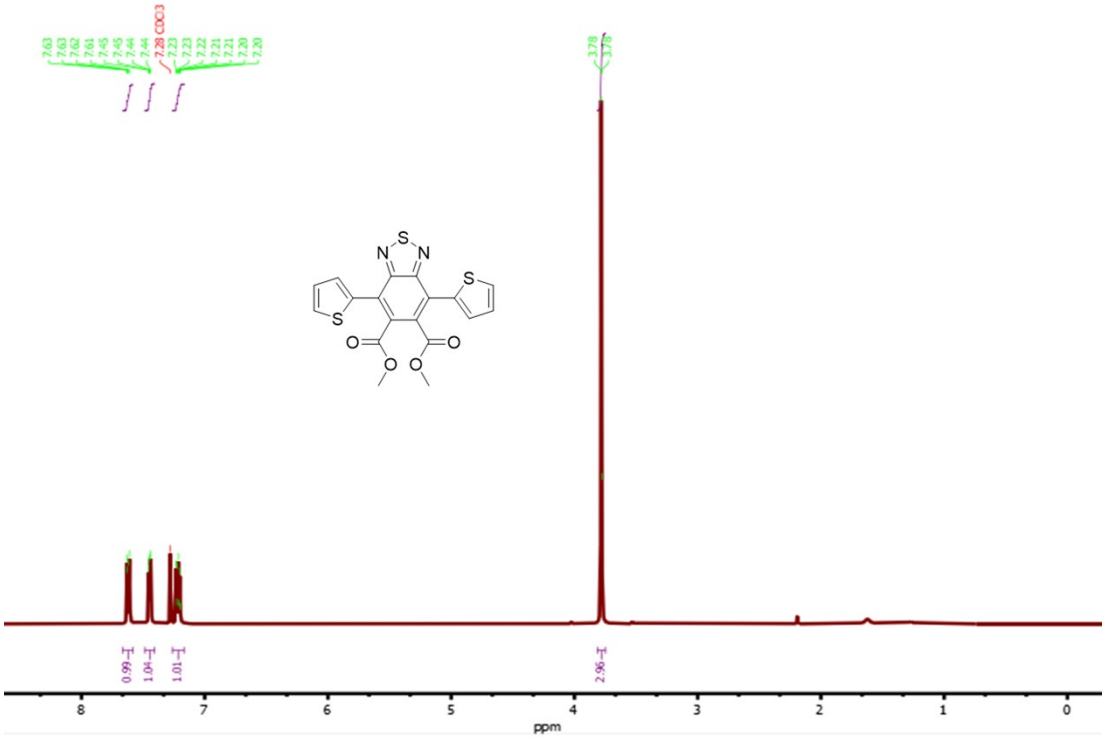

Figure S1. ^{1}HNMR of **DTBTE**.

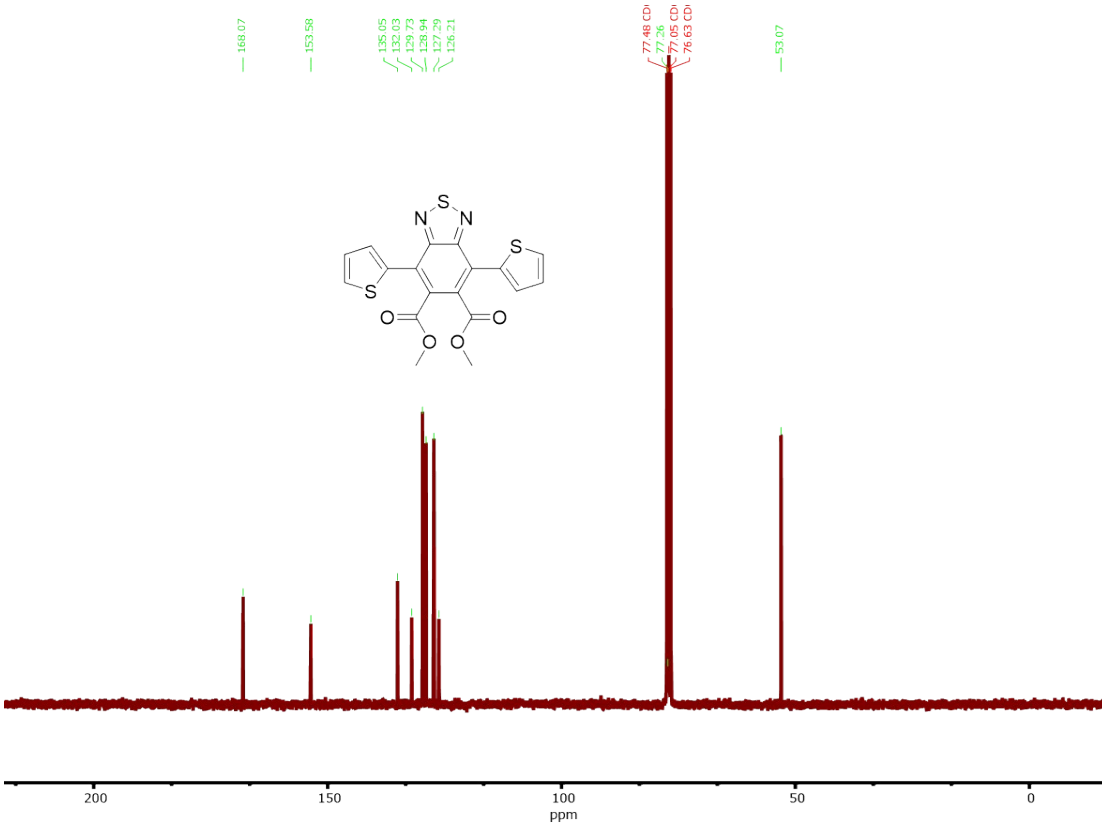

Figure S2. ^{13}CNMR of **DTBTE**.

2. Single crystal X-ray structure determination

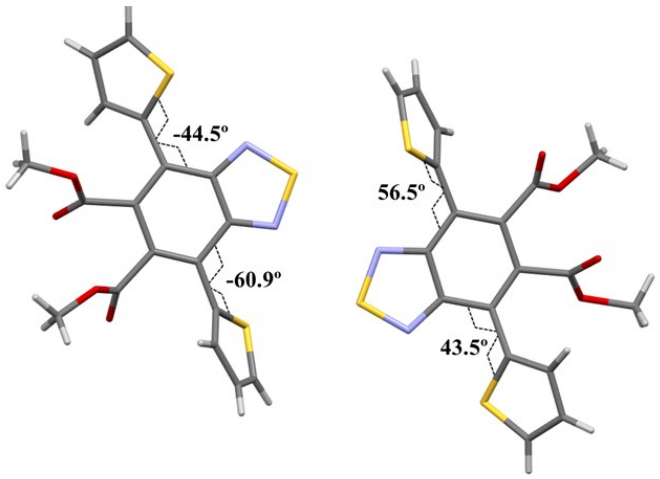

Figure S3. View of the two independent molecules of **DTBTE** in the unit cell.

A suitable crystal of **DTBTE** 0.15×0.05×0.03 mm^3 was selected and placed on a MiTeGen micromount on an Rigaku XtaLAB Synergy- diffractometer with a Cu rotating anode. The crystal was kept at a steady T = 296.00(10) K during data collection. The structure was solved with the SHEXLT [2] structure solution program using the Intrinsic Phasing solution method and by using Olex2 [3] as the graphical interface. The model was refined with of SHELXL[4] using Least Squares minimisation.

Crystal Data. $C_{18}H_{12}N_2O_4S_3$, Mr = 416.48, orthorhombic, $Pna2_1$ (No. 33), a = 20.8691(2) Å, b = 5.97830(10) Å, c = 29.7549(3) Å, α = β = γ = 90°, V = 3712.27(8) Å^3, T = 296.00(10) K, Z = 8, Z' = 2, μ(Cu Kα) = 3.900, 35934 reflections measured, 6772 unique (*Rint* = 0.0320) which were used in all calculations. The final *wR2* was 0.1661 (all data) and *R1* was 0.0526 (I > 2(I)).

CCDC 2415534 contains the supplementary crystallographic data for **DTBTE**. These data can be obtained free of charge via www.ccdc.cam.ac.uk/data_request/cif, or by emailing data_request@ccdc.cam.ac.uk, or by contacting The Cambridge Crystallographic Data Centre, 12 Union Road, Cambridge CB2 1EZ, UK; fax: +44 1223 336033.

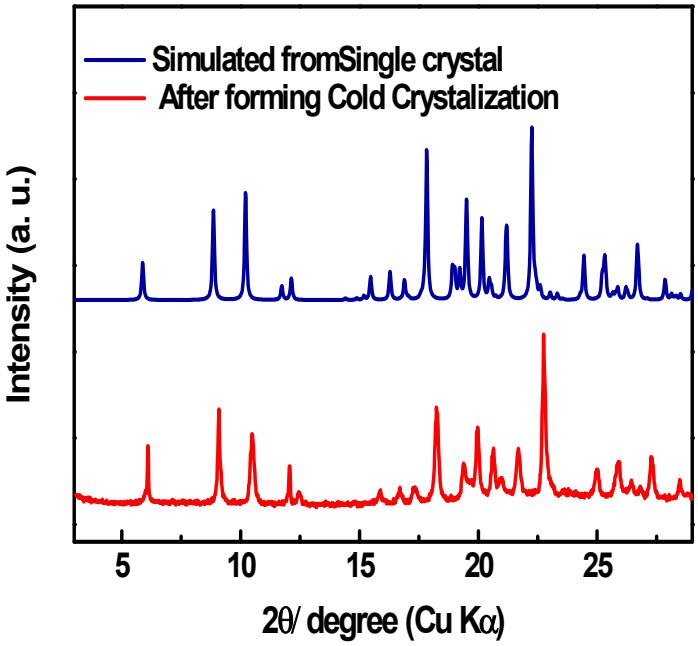

Figure S4. Comparison of powder X-ray diffraction patterns of simulated single crystal from crystal data determination, crystal obtained through cold crystallization.

3. Photophysical characterization

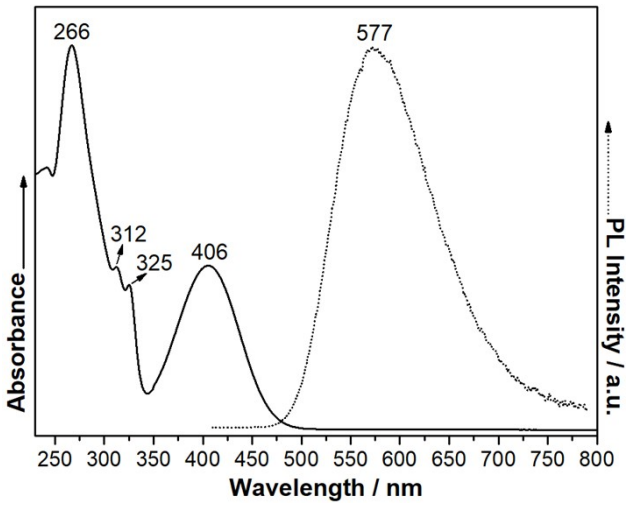

Figure S5. UV−vis absorption (solid line) and fluorescence (dash line) spectra of **DTBTE** in dichloromethane at a concentration of 10^{-4} M. For emission spectrum, an excitation wavelength of 400 nm has been used

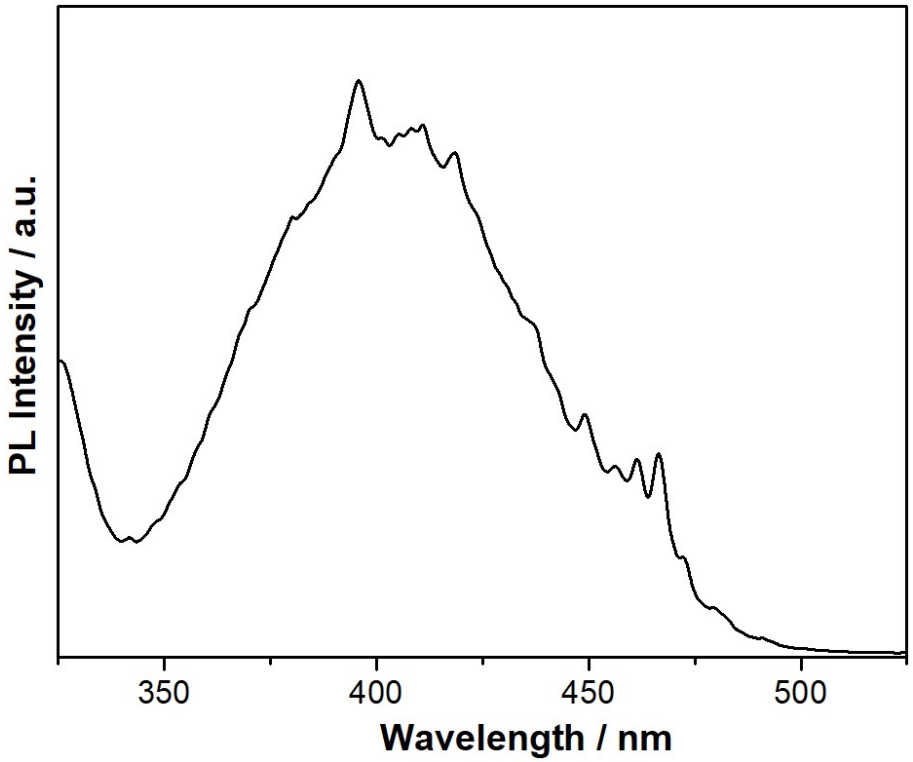

Figure S6. Fluorescence excitation spectra of **DTBTE** in dichloromethane at a concentration of 10^{-4} M (emission at 575 nm).

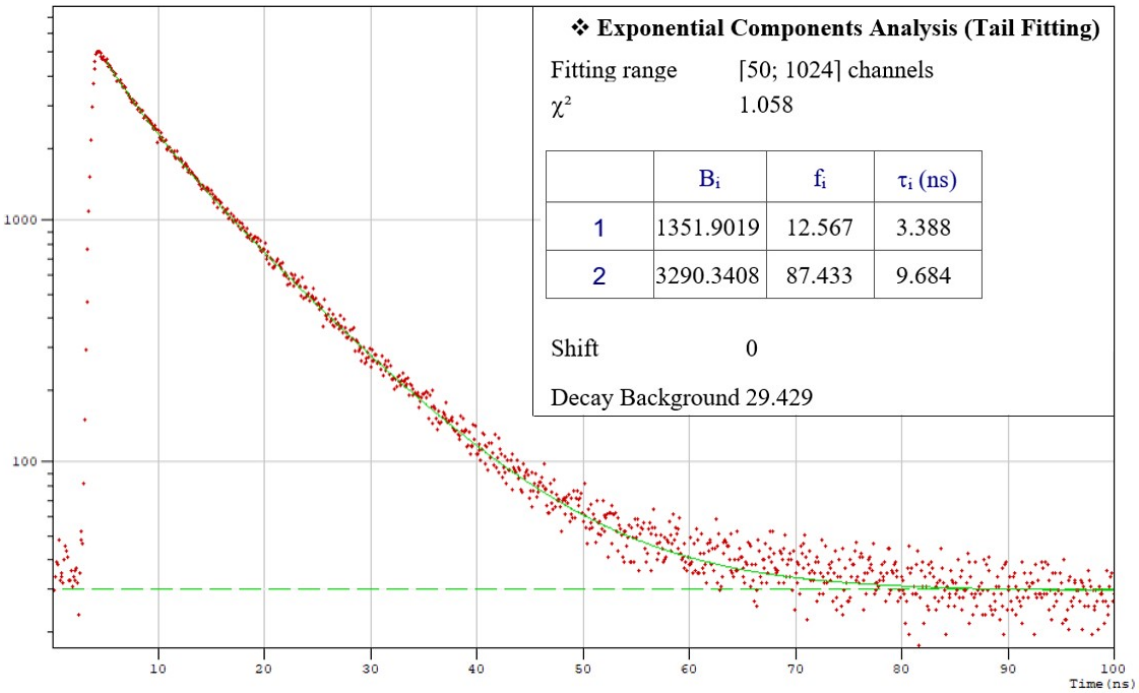

Figure S7. Fluorescence decay of the compound under study solved in dichloromethane. An excitation wavelength of 400 nm has been used.

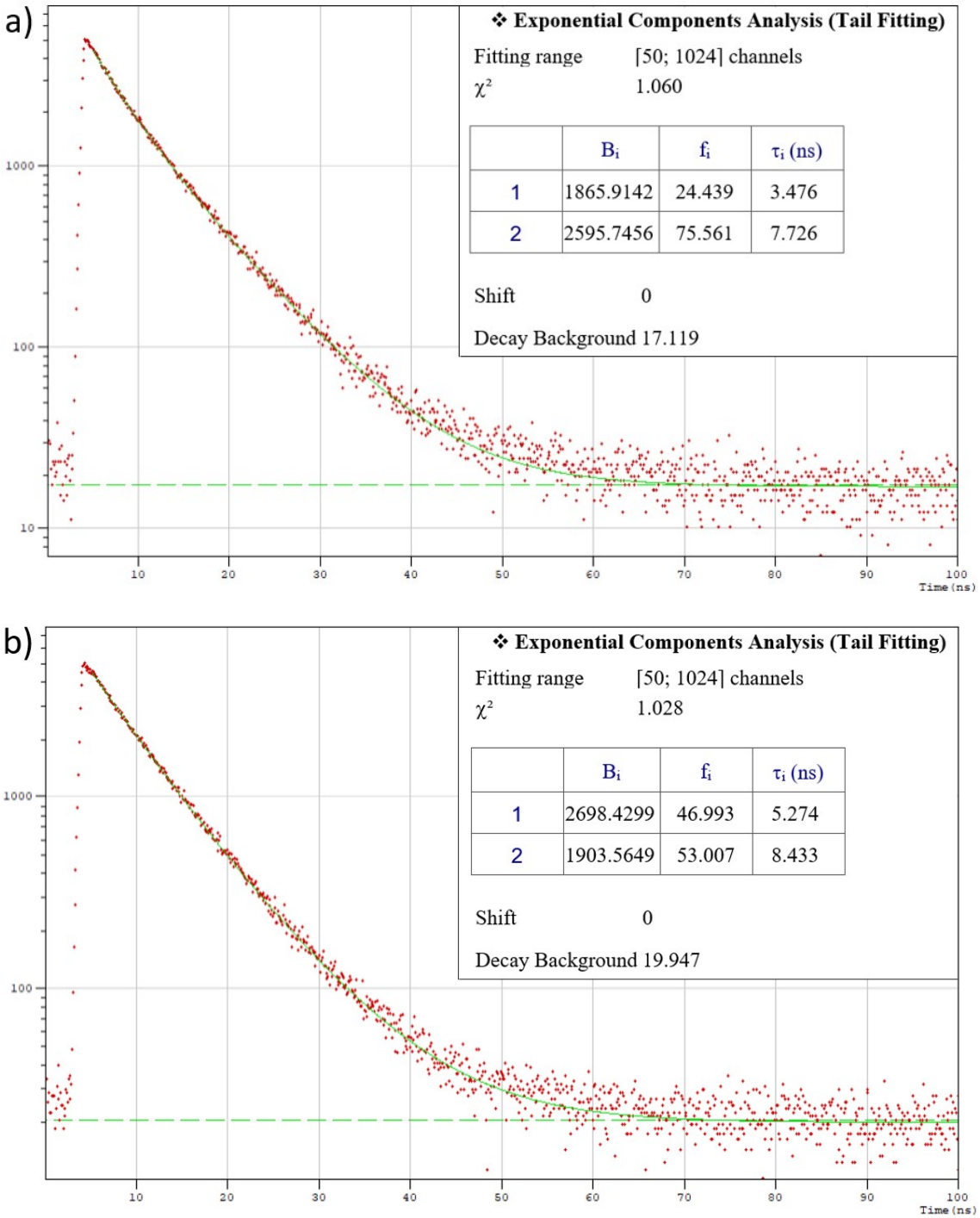

Figure S8. Fluorescence decay of (a) amorphous and (b) crystalline phases of **DTBTE** with an excitation wavelength of 405 nm. Decays show biexponential character.

4. Computational details and DFT calculations

4.1. Computational details

All the calculations were carried out at the framework of the Density Functional Theory (DFT) level using the hybrid, generalized gradient approximation (GGA) functional B3LYP[5], together with the 6-31G** basis set[6], as implemented in the GAUSSIAN16 program[7]. In order to explore the impact of long-range corrections on the structural and optical properties of these systems, the ωB97X-D functional was also used.[8]

As a first step, a preliminary study of the dihedral potential energy hypersurface was performed to further understand the conformational flexibility of this system (see Figures S8 and S9). The relaxed potential energy hypersurface was computed by constraining the angle of the selected dihedral bonds (by step of 10^{o}) and allowing all other degrees of freedom to relax to their potentially energy minima. The resulting potential energy curve was then referenced to the minimal energy structure.

Then, the molecular geometry was fully optimized where all geometrical parameters were allowed to vary independently. Harmonic frequencies calculations were computed, and no imaginary frequencies were observed, which ensures the finding of the global minimum energy.

Vertical electronic excitation energies were calculated by using the time-dependent DFT (TD-DFT)[9] approach on the resulted molecular geometries. Absorption spectra were simulated through convolution of the vertical transition energies and oscillator strengths with Gaussian functions (half width at half-maximum of 0.3 eV).

Simulated Raman spectra for an isolated molecule of **DTBTE** were calculated at the ωB97X-D/6-31G** level. Raman frequencies were scaled down by a factor of 0.946 by using an adjustment of the theoretical force fields to disentangle experimental misassignments, as recommended by Scott and Random. [10] The theoretical spectra were obtained by convolution the scaled frequencies and the Raman activities with Gaussian functions (5 cm^{-1} widths at the half-height).

Molecular orbitals distribution and vibrational eigenvectors were plotted using the Chemcraft 1.8 molecular modelling software. [11]

4.2. DFT and TD-DFT calculations

A) Simulated Absorption Spectra

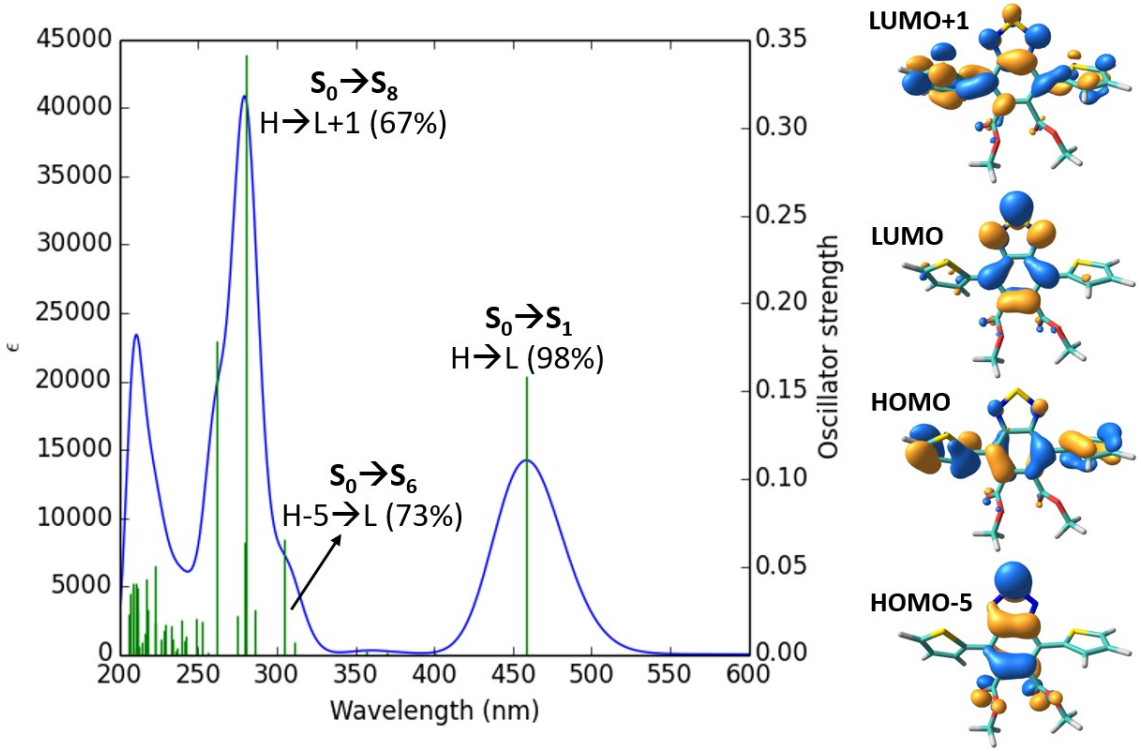

Figure S9. TD-DFT simulated absorption spectrum together with the vertical electronic transitions (green solid bars) at the B3LYP/6-31G** level for the optimized **DTBTE** molecule in a *cis-cis* conformation. The frontier molecular orbitals topologies involved in the main electronic transitions are also shown. Note that H and L denotes HOMO and LUMO, respectively.

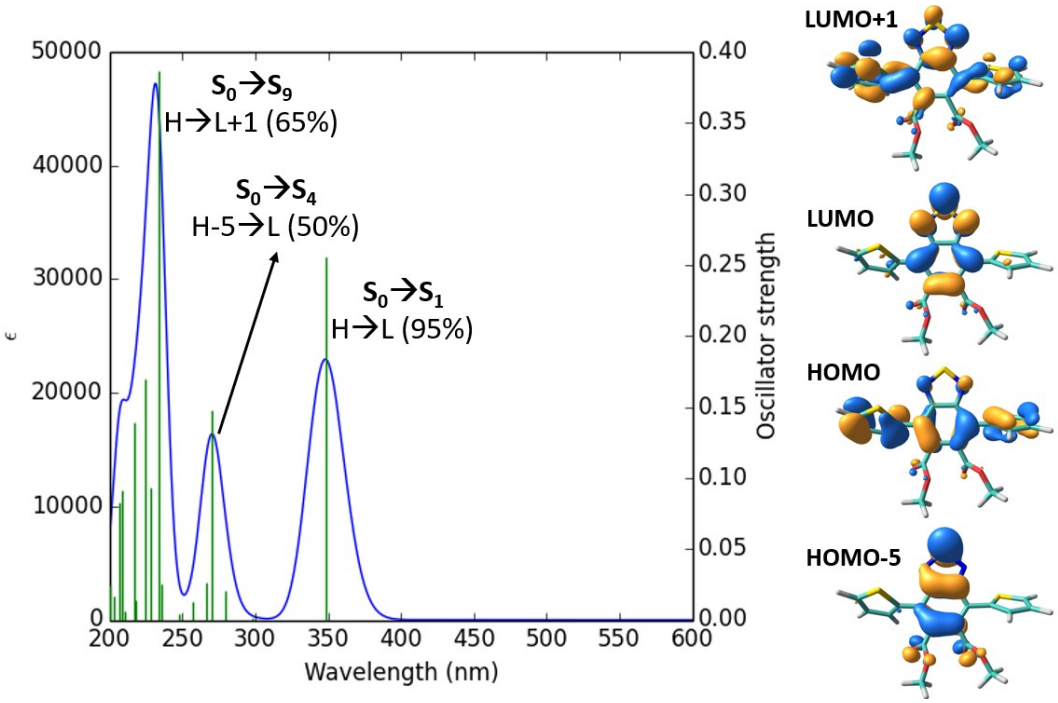

Figure S10. TD-DFT simulated absorption spectrum together with the vertical electronic transitions (green solid bars) at the ωB97X-D/6-31G** level for the optimized **DTBTE** molecule in a *cis-cis* conformation. The frontier molecular orbitals topologies involved in the main electronic transitions are also shown. Note that H and L denotes HOMO and LUMO, respectively.

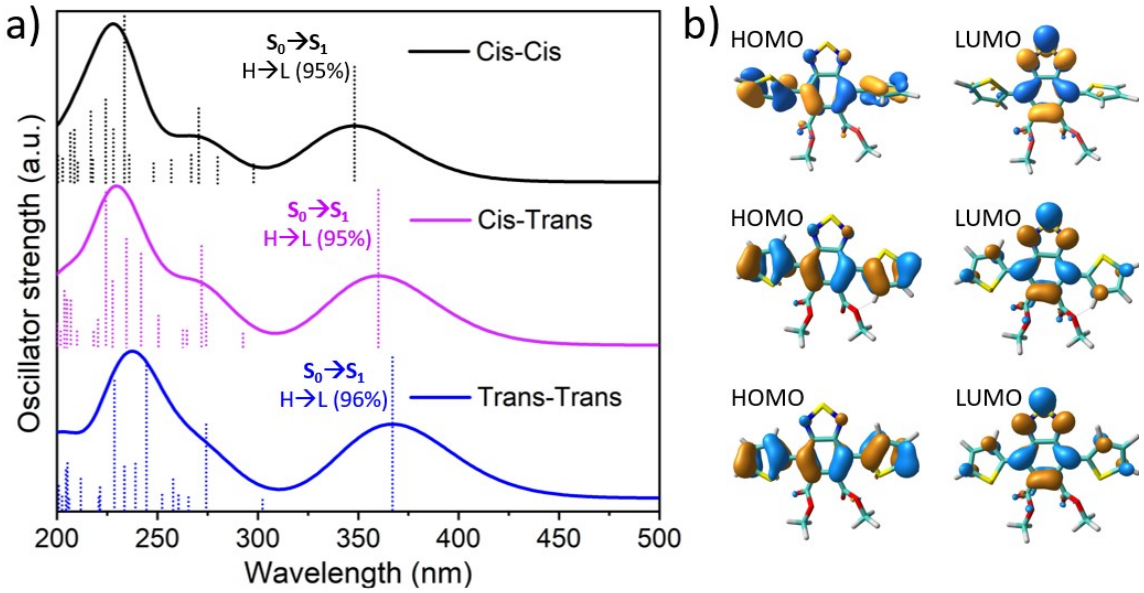

Figure S11. (a) TD-DFT simulated absorption spectrum together with the vertical electronic transitions (dashed lines) for the three possible conformations of **DTBTE**, calculated at the ωB97X-D/6-31G** level of theory. Note that H and L denotes HOMO and LUMO, respectively. (b) HOMO and LUMO topologies, which are primarily involved in the $S_0 \rightarrow S_1$ electronic transitions, for the three possible conformations of **DTBTE**.

B) Conformational Analysis

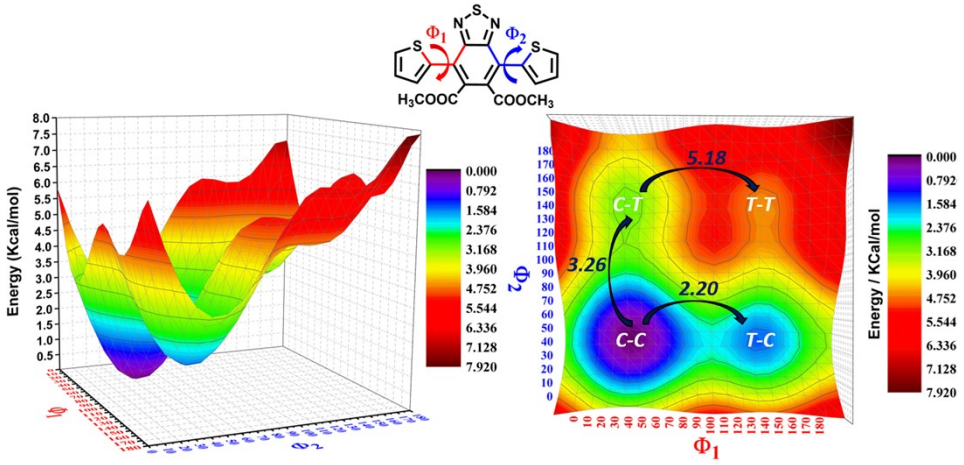

Figure S12. Dihedral potential energy hypersurface relative to the rotations of the thiophene rings with respect to the BTD moiety (ϕ_1,ϕ_2) calculated for an isolated **DTBTE** molecule at the B3LYP/6-31G** level of theory. The four possible conformers (white letters) and the energetic barriers between them are also shown.

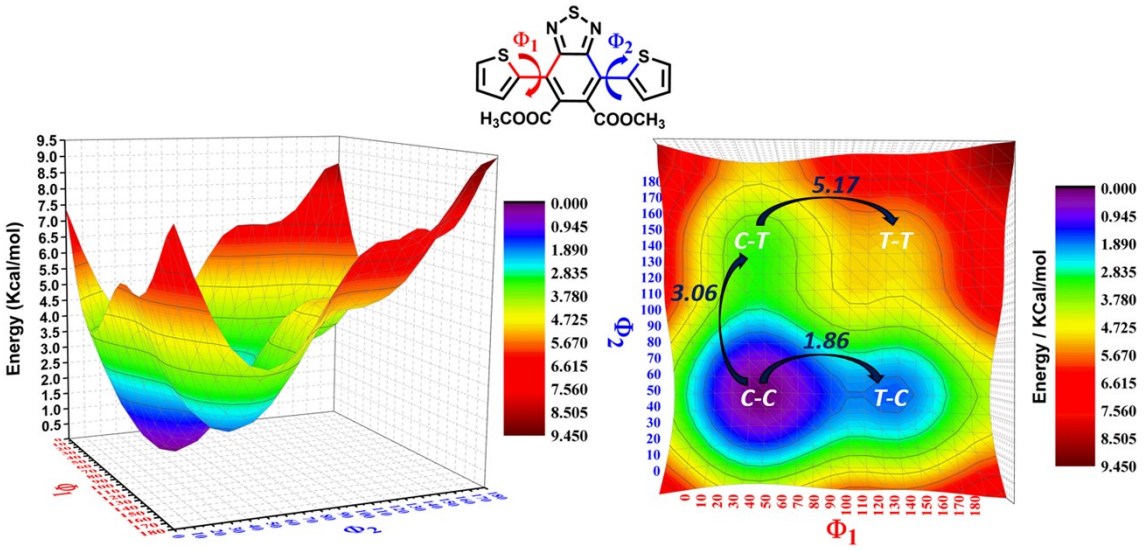

Figure S13. Dihedral potential energy hypersurface relative to the rotations of the thiophene rings with respect to the BTD moiety (ϕ_1,ϕ_2) calculated for an isolated **DTBTE** molecule at the ωB97X-D/6-31G** level of theory. The four possible conformers (white letters) and the energetic barriers between them are also shown.

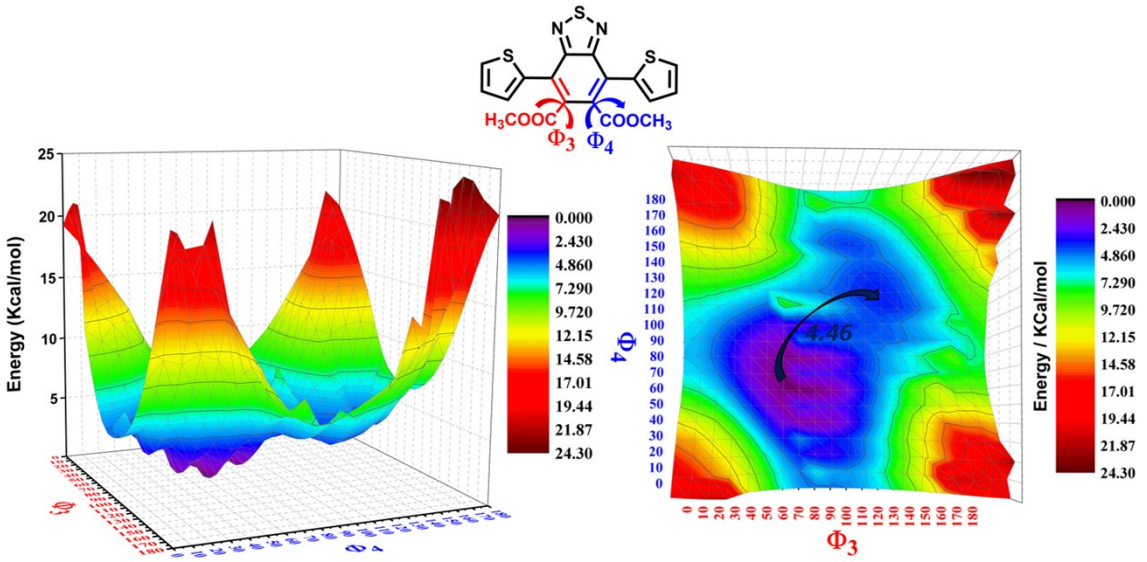

Figure S14. Dihedral potential energy hypersurface relative to the rotations of the carbonyl ester groups with respect to the BTD moiety (ϕ_3,ϕ_4) calculated for an isolated **DTBTE** molecule at the B3LYP/6-31G** level of theory.

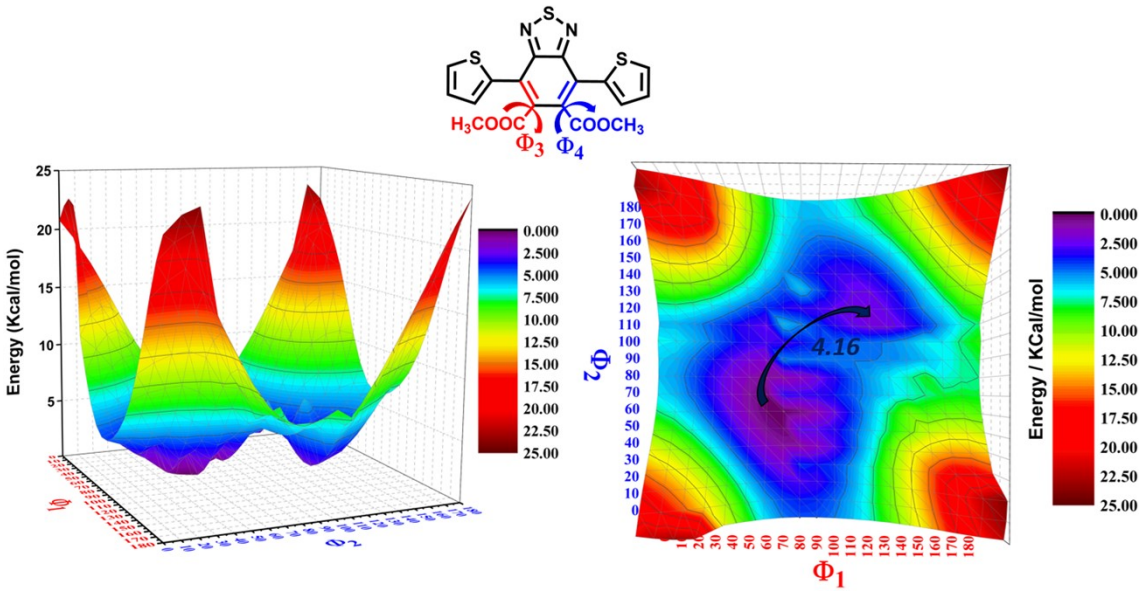

Figure S15. Dihedral potential energy hypersurface relative to the rotations of the carbonyl ester groups with respect to the BTD moiety (ϕ_3,ϕ_4) calculated for an isolated **DTBTE** molecule at the ωB97X-D/6-31G** level of theory.

C) Molecular Structural Parameters

	Exp. Data*	B3LYP/6-31G**	ωB97X-D/6-31G**
ϕ_1	57° (61°)	61°	64°
ϕ_2	44° (45°)	49°	53°
ϕ_3	55° (57°)	60°	57°
ϕ_4	58° (60°)	67°	69°

Figure S16. Comparison between the DFT-optimized dihedral angle values for the **DTBTE** system in a *cis-cis* conformation and those obtained experimentally. *Since the experimentally determined structure contains two molecules on the unit cell, two dihedral angle values are shown.

a)

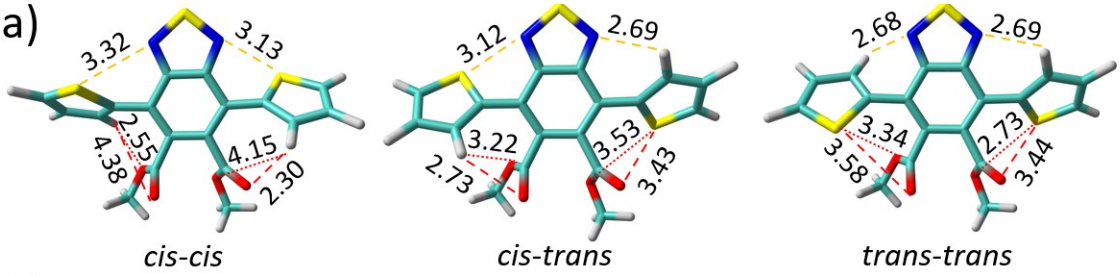

cis-cis *cis-trans* *trans-trans*

b)

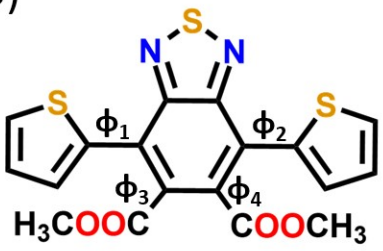

	B3LYP/6-31G**		
	cis-cis	***cis-trans***	***trans-trans***
ϕ_1	61°	46° (*trans*)	43°
ϕ_2	49°	44°	43°
ϕ_3	60°	61° (*trans*)	60°
ϕ_4	67°	65°	63°

Figure S17. (a) Lateral views of the optimized geometries for the three possible conformations of **DTBTE**, calculated at the B3LYP/6-31G** level of theory. Key intramolecular distances (S-N, H-N, S-O and H-O) are annotated in Å. (b) Comparison of the DFT-optimized dihedral angle values for the three conformations of **DTBTE**, calculated at the same level of theory.

a)

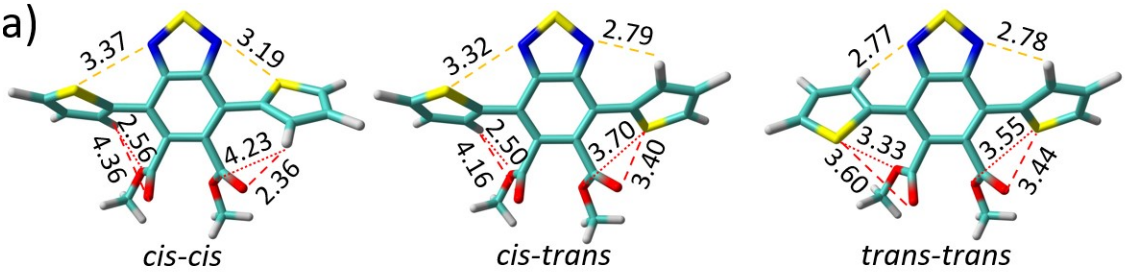

b)

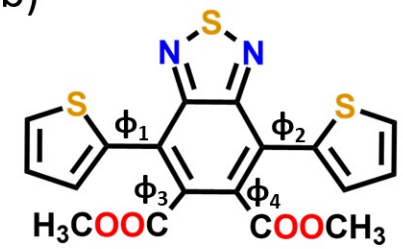

	ωB97X-D/6-31G**		
	cis-cis	***cis-trans***	***trans-trans***
ϕ_1	64°	47° (*trans*)	47°
ϕ_2	53°	59°	47°
ϕ_3	57°	52° (*trans*)	59°
ϕ_4	69°	76°	61°

Figure S18. (a) Lateral views of the optimized geometries for the three possible conformations of **DTBTE**, calculated at the ωB97X-D/6-31G** level of theory. Key intramolecular distances (S-N, H-N, S-O and H-O) are annotated in Å. (b) Comparison of the DFT-optimized dihedral angle values for the three conformations of **DTBTE**, calculated at the same level of theory.

5. Raman analysis

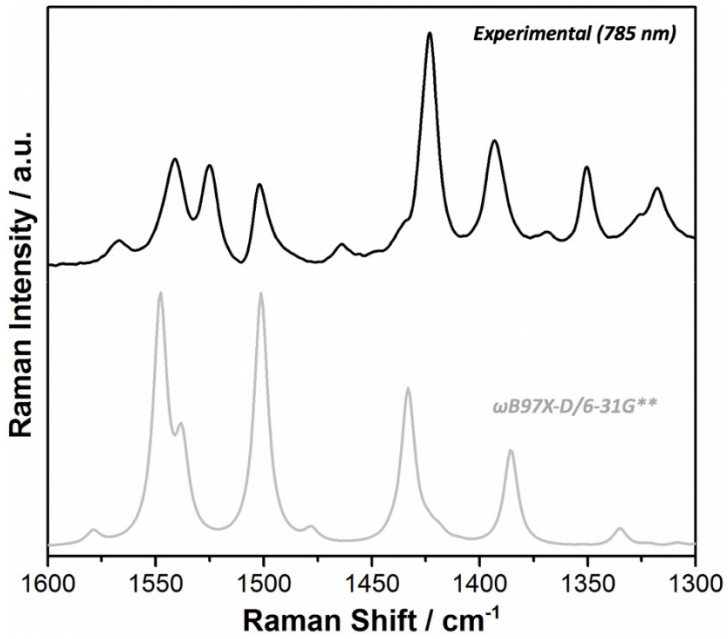

Figure S19. Comparison of the Raman spectrum of **DTBTE** in the crystalline state with the DFT-Calculated spectrum (at the ωB97X-D/6-31G** level) for the optimized molecular structure.

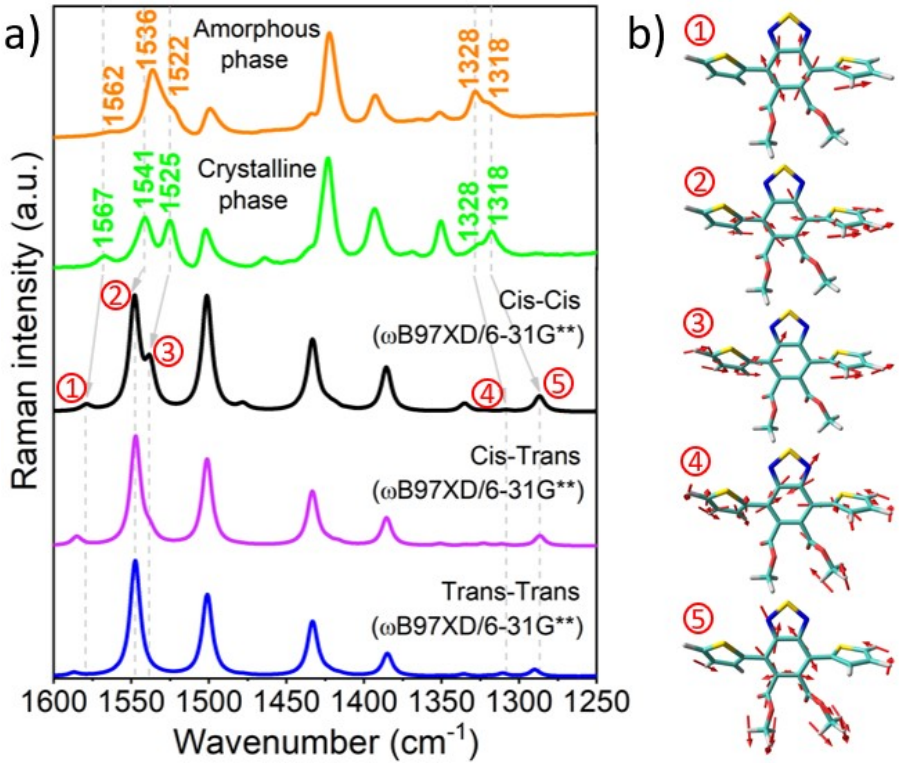

Figure S20. (a) Comparison of the Raman spectra of **DTBTE** in the amorphous (orange line) and crystalline (green line) phases with the DFT-predicted spectra (ωB97X-D/6-31G**) for its three possible conformations. (b) Vibrational eigenvectors associated with the highlighted Raman bands.

6. IR analysis

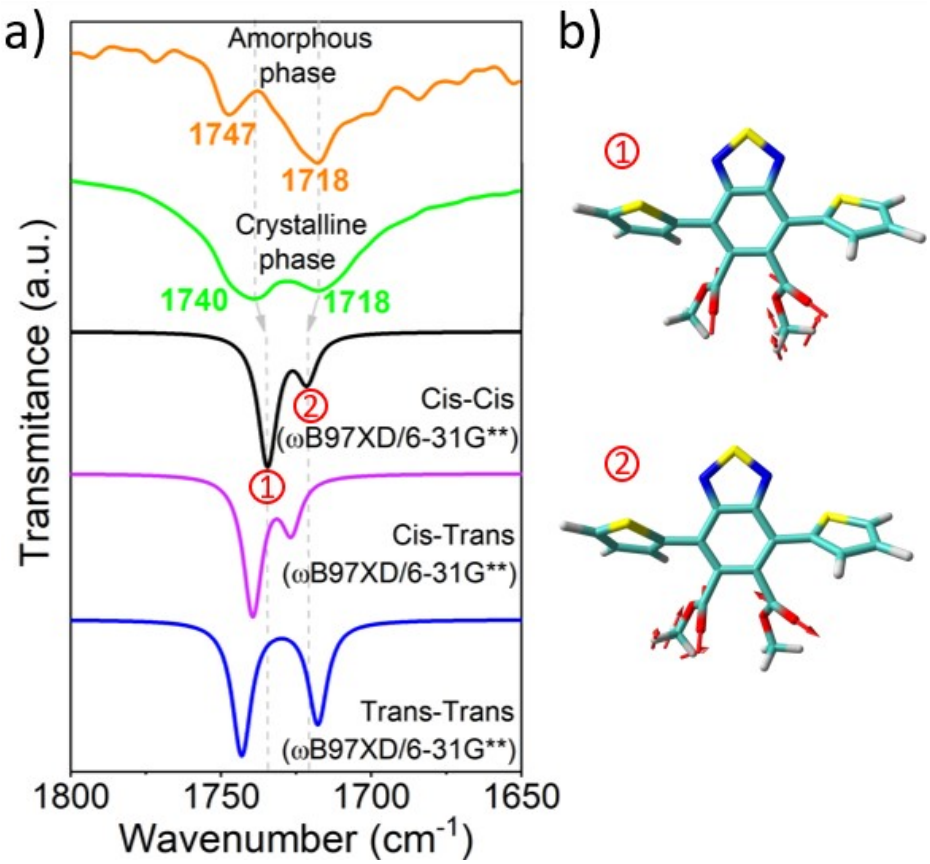

Figure S21. (a) Comparison of the IR spectra of **DTBTE** in the amorphous (orange line) and crystalline (green line) phases with the DFT-predicted spectra (ωB97X-D/6-31G**) for its three possible conformations in the 1800-1650 cm^{-1} spectral region. (b) Vibrational eigenvectors associated with the highlighted IR bands.

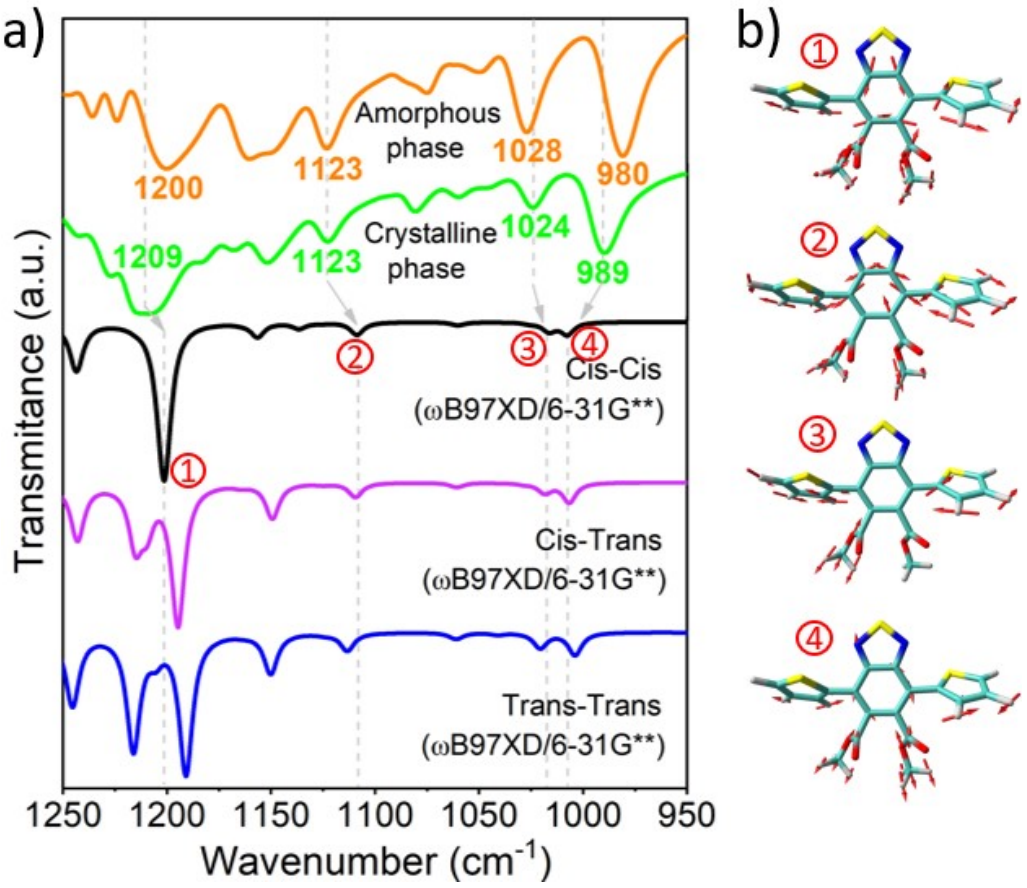

Figure S22. (a) Comparison of the IR spectra of **DTBTE** in the amorphous (orange line) and crystalline (green line) phases with the DFT-predicted spectra (ωB97X-D/6-31G**) for its three possible conformations in the 1250-950 cm^{-1} spectral region. (b) Vibrational eigenvectors associated with the highlighted IR bands.

7. Scanning Electron Microscopy (SEM) images

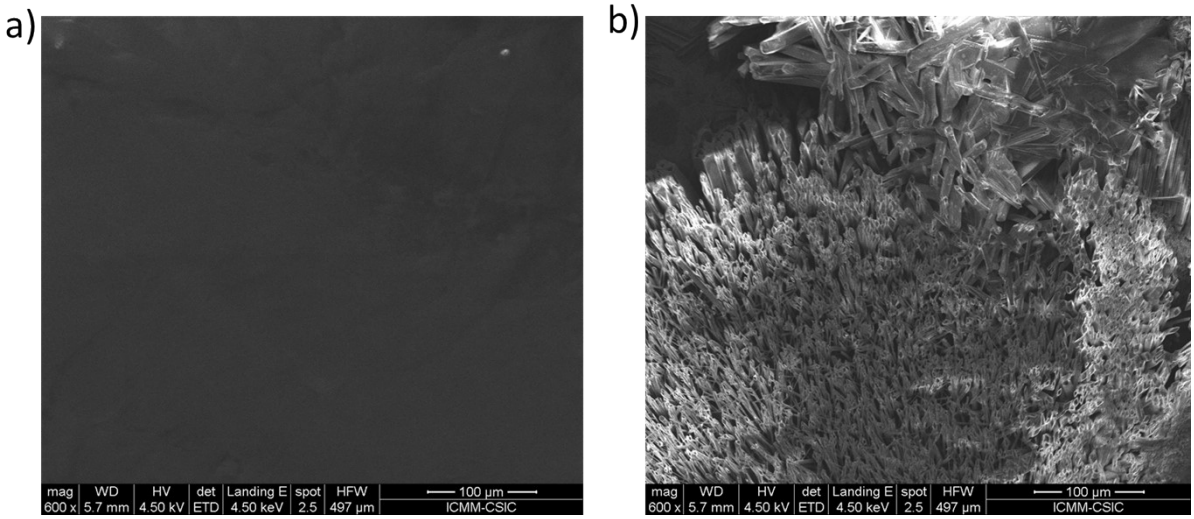

Figure S23. SEM images of at 100 µm magnification (a) as cast **DTBTE** film and (b) after thermal annealing of **DTBTE** film at 80 ºC.

8. Stimuli-responsive luminiscence

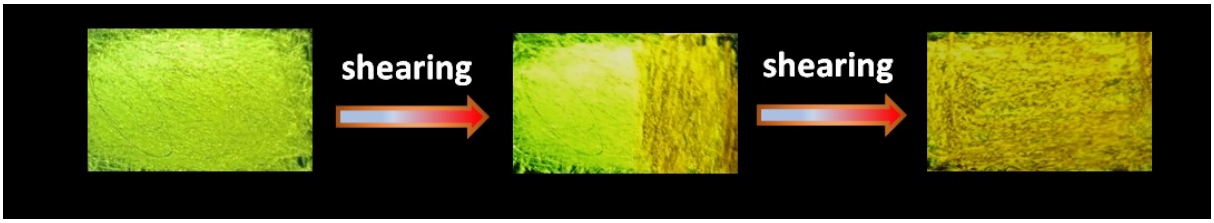

Figure S24. Illustration of the mechanohromic behavior induced by shearing a **DTBTE** film on a glass slide with a spatula, visualized under a UV lamp (356 nm).

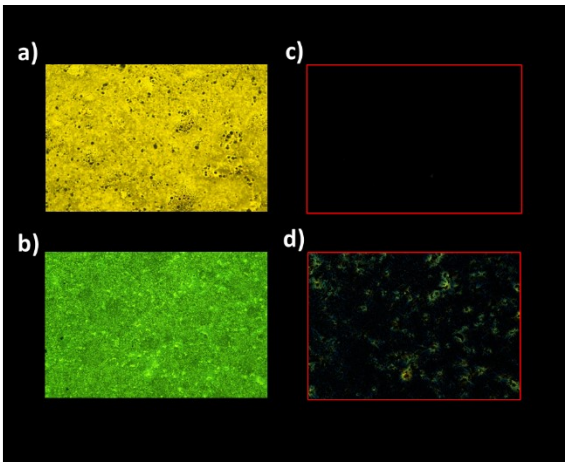

Figure S25. Microscopic images of the textures of an (a,c) as-cast and (b,d) heated (80 °C for 1h) **DTBTE** film on glass, visualized under (a,b) 356 nm UV light and under (c,d) crossed polarizers.

Figure S26. Colored paper utilizing a THF solution of **DTBTE** (0.5 wt.%) as ink, illustrating reversible color emission changes. The transformation after heating and subsequently recovery upon exposure to CH_2Cl_2 vapors is observed under a UV lamp (356 nm).

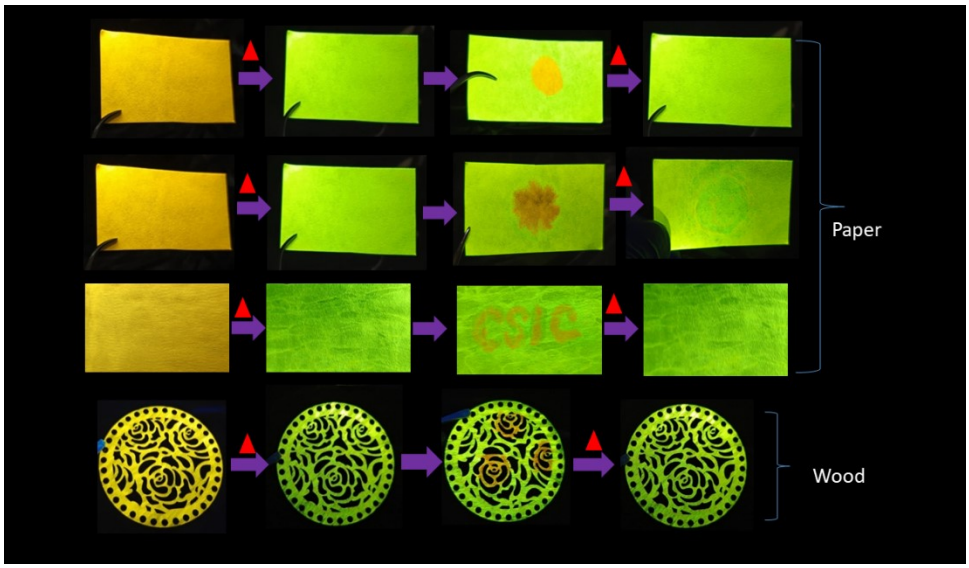

Figure S27. Decoration and message written on paper and wood utilizing a **DTBTE** (0.5 wt.%) solution in THF as ink, demonstrating reversible color emission changes. The transformation after heating and subsequently recovery upon exposure to CH_2Cl_2 vaporsis visualized under a UV lamp (356 nm).

9. References

1. (a) Lan, L.; Chen, Z.; Hu, Q.; Ying, L.; Zhu, R.; Liu, F.; Russell, T. P. ; Huang, F. and Cao, Y., High-Performance Polymer Solar Cells Based on a Wide-Bandgap Polymer Containing Pyrrolo[3,4-f]benzotriazole-5,7-dione with a Power Conversion Efficiency of 8.63%. *Adv. Sci.* **2016**, *3*, 1600032; (b) Abdulahi, B. A.; Li, X.; Mone, M.; Kiros, B.; Genene, Z.; Qiao, S.; Yang, R.; Wang E.and Mammo, W., Structural engineering of pyrrolo[3,4-f]benzotriazole-5,7(2H,6H)-dione-based polymers for non-fullerene organic solar cells with an efficiency over 12%. *J. Mater. Chem. A,* **2019***,7,* 19522-19530.
2. Sheldrick, G. M. C SHELXT - Integrated Space-group and Crystal-structure Determination, *Acta Crystallogr. A Struct. Chem.* **2015**, *71*, 3–8.
3. Dolomanov O.V.; Bourhis L.J.; Gildea R.J.; Howard J.A.K. Puschmann, H., Olex2: A complete structure solution, refinement and analysis program, *J. Appl. Cryst.*, **2009**, *42*, 339-341.
4. Sheldrick, G. M. Crystal Structure Refinement with SHELXL, *Acta Crystallogr. C Struct. Chem.* **2015**, *71*, 3–8
5. (a) Lee, C.; Yang, W.; Parr, R. G., Development of the Colle-Salvetti correlation-energy formula into a functional of the electron density. *Phys. Rev. B* **1988,** *37* (2), 785-789; (b) Becke, A. D., Density-functional thermochemistry. III. The role of exact exchange. *J. Chem. Phys.* **1993,** *98* (7), 5648-5652.
6. (a) Hehre, W. J.; Ditchfield, R.; Pople, J. A., Self—Consistent Molecular Orbital Methods. XII. Further Extensions of Gaussian—Type Basis Sets for Use in Molecular Orbital Studies of Organic Molecules. *J. Chem. Phys.* **1972,** *56* (5), 2257-2261; (b) Francl, M. M.; Pietro, W. J.; Hehre, W. J.; Binkley, J. S.; Gordon, M. S.; DeFrees, D. J.; Pople, J. A., Self-consistent molecular orbital methods. XXIII. A polarization-type basis set for second-row elements. *J. Chem. Phys.* **1982,** *77* (7), 3654-3665.
7. M. J. Frisch, G. W. T., H. B. Schlegel, G. E. Scuseria, M. A. Robb, J. R. Cheeseman, G. Scalmani, V. Barone, G. A. Petersson, H. Nakatsuji, X. Li, M. Caricato, A. V. Marenich, J.

Bloino, B. G. Janesko, R. Gomperts, B. Mennucci, H. P. Hratchian, J. V. Ortiz, A. F. Izmaylov, J. L. Sonnenberg, D. Williams-Young, F. Ding, F. Lipparini, F. Egidi, J. Goings, B. Peng, A. Petrone, T. Henderson, D. Ranasinghe, V. G. Zakrzewski, J. Gao, N. Rega, G. Zheng, W. Liang, M. Hada, M. Ehara, K. Toyota, R. Fukuda, J. Hasegawa, M. Ishida, T. Nakajima, Y. Honda, O. Kitao, H. Nakai, T. Vreven, K. Throssell, J. A. Montgomery, Jr., J. E. Peralta, F. Ogliaro, M. J. Bearpark, J. J. Heyd, E. N. Brothers, K. N. Kudin, V. N. Staroverov, T. A. Keith, R. Kobayashi, J. Normand, K. Raghavachari, A. P. Rendell, J. C. Burant, S. S. Iyengar, J. Tomasi, M. Cossi, J. M. Millam, M. Klene, C. Adamo, R. Cammi, J. W. Ochterski, R. L. Martin, K. Morokuma, O. Farkas, J. B. Foresman, and D. J. Fox. , Gaussian 16, Revision B.01. *Gaussian, Inc., Wallingford CT,* **2016**.

8. Chai, J.-D.; Head-Gordon, M., Long-range corrected hybrid density functionals with damped atom–atom dispersion corrections. *Phys. Chem. Chem. Phys.* **2008,** *10* (44), 6615-6620.

9. (a) Runge, E.; Gross, E. K. U., Density-Functional Theory for Time-Dependent Systems. *Phys. Rev. Lett.* **1984,** *52* (12), 997-1000; (b) Heinze, H. H.; Görling, A.; Rösch, N., An efficient method for calculating molecular excitation energies by time-dependent density-functional theory. *J. Chem. Phys.* **2000,** *113* (6), 2088-2099.

10. Scott, A. P.; Radom, L., Harmonic Vibrational Frequencies: An Evaluation of Hartree−Fock, Møller−Plesset, Quadratic Configuration Interaction, Density Functional Theory, and Semiempirical Scale Factors. *J. Phys. Chem.* **1996,** *100* (41), 16502-16513.

11. https://www.chemcraftprog.com, Chemcraft - graphical software for visualization of quantum chemistry computations.